Dechanneling of protons in diamond

R. W. Fearick, T. E. Derry, and J. P. F. Sellschop
Schonland Research Centre for Nuclear Sciences, University of the Witwatersrand, Johannesburg, P.O. Wits 2050, South Africa
(Received 9 November 1988; revised manuscript received 26 April 1989)

The axial dechanneling of protons in natural diamond crystals selected for low defect levels has been studied for beam energies of 1.0–8.9 MeV and crystal temperatures from 20–600 °C. Measurements of the dechanneled-ion yield were taken along the three major axes ⟨110⟩, ⟨111⟩, and ⟨100⟩. The data have been analyzed in terms of the diffusion model of dechanneling and generally good agreement between experiment and theory is obtained. The theory indicates that the predominant contribution to the dechanneling is from the electronic scattering. A scaling of the energy-dependent data for a given axis with a distance characteristic of the electronic scattering is observed. This scaling holds approximately for all data in the three axes considered. Measurements of the yield as a function of temperature indicate that the theory underestimates the nuclear scattering.

I. INTRODUCTION

The dechanneling of ions in crystals has been studied for a number of years[1–6] and it is understood that the transition from a channeled to a random state of motion in a perfect crystal is brought about by the scattering of the channeled ion by electrons in the crystal (electronic scattering) and by the fluctuating force resulting from the thermal motion of the crystal atoms (nuclear scattering). The rate of dechanneling is determined by the combination of these effects, and depends on the energy of the ion and the temperature of the crystal, as well as the atomic numbers and masses of the ion and crystal atoms. While it is not in general possible to separate these two dechanneling mechanisms, some understanding of their individual effects can be obtained by studying cases in which one or the other is favored. Most dechanneling studies heretofore have been on crystals in which the thermal (nuclear) mechanism is dominant. In this paper, we report results for dechanneling in diamond. Diamond has a low atomic number and a high Debye temperature [1860 K (Ref. 7)]—both of these result in reducing the importance of nuclear scattering. In addition the valence electron density in diamond, which is important in electronic scattering, is relatively high. Thus, it is expected that electronic scattering is important in the case of diamond.

In order to explore this, we have studied the axial dechanneling of protons in selected natural diamonds, with beam energies ranging from 1.0 to 8.9 MeV, and crystal temperatures from room temperature (20 °C) to 600 °C. The data have been interpreted in terms of the diffusion model[3–6] of dechanneling. The analysis has demonstrated the relative importance of electronic scattering in the case of diamond.

The change with depth of the yield of a close-encounter process such as backscattering is a complex function of energy, temperature, and crystal direction, and the question arises whether it can be described by some combination of these parameters, i.e., by some scaling law. Several workers[2,8,9] have suggested that the yield should depend on the variable u_2/E, where u_2 is the root-mean-square thermal vibration amplitude of the crystal atoms in two dimensions, and E is the ion energy. Such a relationship has not been observed by other authors.[6,10] We have determined that, in diamond, the yield scales approximately with a length z_e characteristic of the electronic scattering. The scaling is broken by the somewhat different energy dependence of the nuclear scattering and, to a lesser extent, by the effects of large-angle scattering and of damping (i.e., the effect on the dechanneling process of the energy loss of the ion). Nevertheless, the yield is determined approximately by one parameter over a wide range of energy and temperature. This scaling also extends, to some extent, to other axes. This somewhat surprising observation can be understood in terms of the diffusion model of dechanneling. While the initial transverse energy distributions of the ions in the three axes studied are quite different, leading to different surface minimum yields, these differences are washed out by the diffusion process and a similar behavior is observed at some depth into the crystal.

II. EXPERIMENTAL ASPECTS AND DATA ANALYSIS

The experiments were performed at the Schonland Research Center for Nuclear Sciences (formerly the N.P.R.U.) of the University of the Witwatersrand. Two accelerators were used; a pressurized Cockcroft-Walton accelerator was used for the 1.0-MeV measurements, and an EN tandem van de Graaff accelerator was used for higher-energy measurements. Similar experimental arrangements were used on both accelerators. The target crystal was mounted in a two-axis goniometer driven by stepping motors, with an angular precision of 0.01°. The proton beam was collimated to 0.2 mrad divergence on the low-energy accelerator, and to 0.02 mrad on the high-energy accelerator, by means of a system of adjustable slits and apertures. Backscattered protons were detected at a laboratory angle of 155.0° in a silicon

surface-barrier detector with an energy resolution of 14 keV. The detector was mounted in the plane defined by the incident beam and the goniometer tilt axis, so that the energy to depth conversion for scattered protons was independent of the goniometer setting. The target chambers were pumped by means of turbopumps, and shields cooled by liquid nitrogen surrounded the target in order to reduce contamination. Pressures during the experimental runs were of the order of 10^{-6} torr, and observed rates of deposition of impurities on the targets were low, as judged from the surface peak observed in the channeled spectra, and the presence of higher-energy peaks in the spectra. The predominant contaminants were carbon and oxygen, and the surface coverage was at most a few monolayers. The effect of this on channeling was judged to be minimal. A filament arrangement was used to supply electrons to the crystal in order to prevent target charging, which had been observed to deflect the incident beam slightly by an amount dependent upon the target current at large goniometer tilt angles. The entire target chamber was insulated from ground and used as a Faraday cage for beam current integration. Measurements were also taken at 1.0 MeV of the temperature dependence of dechanneling, using a resistive heater in contact with the target holder. The temperature was measured with a thermocouple sandwiched between the heater and the target holder.

The crystals used were natural type-I*a* diamonds with a low concentration of platelets. These were expected from other studies[11] to be the most perfect diamond crystals for channeling purposes. The crystals were polished to a high degree of surface finish using standard diamond polishing techniques and were cleaned in solvents and detergents before use.[12] This technique of surface preparation has been found to give good surfaces with no effect in backscattered spectra that could be ascribed to surface damage. These good results are presumably due to the special mechanisms involved in the polishing of diamond. The surface peak in a ⟨110⟩ channeled spectrum for 1.0-MeV protons typically corresponded to 6–8 monolayers (ML) of carbon; a Monte Carlo simulation of such scattering gave approximately 4 ML.

Spectra in both channeled and random orientation were accumulated for a fixed beam fluence, usually 1.2 μC. Random spectra were taken while rotating the crystal about the axial direction, with the crystal offset from the channeled direction by a few degrees (about $10\psi_1$). This procedure gave consistent results for several offset angles while the technique of selecting a particular direction far from the major axis and accumulating a spectrum at fixed goniometer angles did not. Other methods of obtaining a random spectrum, e.g., by using an amorphous target, were not tried, as the stopping power of protons in carbon, and hence the height of the random spectrum, is known[13] to depend on the nature of bonding in different carbon allotropes.

The scattering cross section for protons on carbon is non-Rutherfordian even at 1.0 MeV, and at higher energies careful selection of incident energy was necessary in order to avoid energy regions with strong resonances. Measurements were thus performed at 1.0, 4.5, 7.0, and 8.9 MeV. Figure 1 shows a random and a ⟨110⟩ channeled spectrum at 1.0 MeV. The cross section varies slowly over the path of the incident ion before scattering, and thus the shape of the random spectrum is determined largely by the stopping power; this leads to the strong dip at low energies corresponding to the peak in the stopping power.

Channeled spectra were normalized to random by dividing channel by channel with the random spectrum. This method ignores any difference in energy loss between channeled and random ions.[4] In addition, random energy loss was used to assign a depth scale to the spectra. We feel that this procedure is justified for several reasons. The energy loss of an ion from the surface to a certain depth will depend on the exact path followed by the ion, and using, as is often suggested, a channeled ion stopping power which is a fixed fraction of the random stopping power, will not give correct results for all ions. The fraction to be used is not well known in diamond; in addition the fraction to be used will also be depth dependent in a manner which is not easily determined. Also, the shape of the spectrum depends on the stopping power. An analysis of a 1.0 MeV ⟨110⟩ spectrum, assuming that the channeled stopping power is half of the random, shows that the main effect is to change the shape of the yield curve, rather than to raise or lower the yield over the full extent of the curve.

A depth scale was assigned to the spectrum using the stopping power fits of Andersen and Ziegler.[14] There are thus two sources of systematic uncertainty in the assigned depth scales: one from the channeled versus random stopping power problem, and the other due to uncertainties in the stopping power due to the allotropic dependence. The latter effect is expected to be rather small, as measurements[15] of energy loss in thin diamond crystals for (2.5–12.0)-MeV protons showed good agreement with the Andersen and Ziegler values; in addition, calculation of the height of the random spectrum using these stopping power values and the measured cross section at 1.0 MeV gave good agreement with the measured

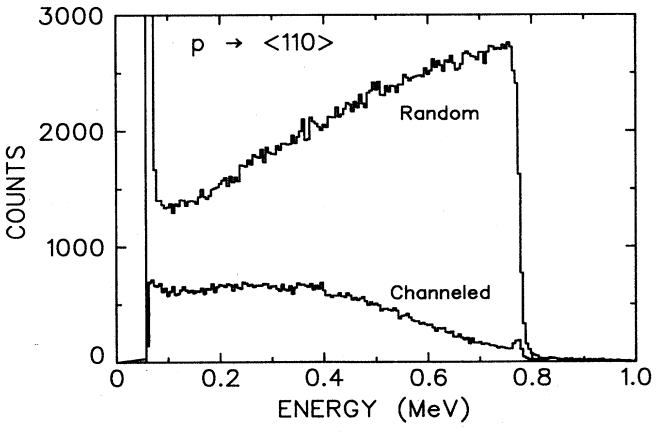

FIG. 1. Random energy spectrum and ⟨110⟩ channeled spectrum for 1.0 MeV protons in diamond.

height. We note that allotropic effects on the stopping power depend largely on the valence electrons and can be expected to be more important at lower energies.[16] Presentation and discussion of the experimental results is postponed to Sec. IV.

III. THEORETICAL DESCRIPTION OF THE YIELD

A. Theory of dechanneling

In order to provide some basis for the evaluation of various contributions to the dechanneled yield, the results were analyzed in terms of the diffusion model of dechanneling.[3-6] We have attempted to make the calculations as accurate as possible, and have thus used more realistic potentials and electron densities than the usual Lindhard[1] or Molière[17] approximations. In addition we have tried to take into account the two-dimensional nature of the transverse plane. Our approach is thus somewhat different from that of other authors, such as Matsunami and Howe,[6] who attempted to find good approximations in order to extend their calculations to more complex damage cases, and thus we summarize in some detail our theoretical approach.

Within the continuum model of channeling the motion of a channeled particle can be described by its motion in the plane transverse to the axis along which channeling occurs. The motion is governed by the transverse energy,

$$E_\perp = p_\perp^2/2m + U(\mathbf{r}) ,$$

where $\mathbf{p}_\perp$ is the transverse momentum of the ion at $\mathbf{r}$ in the transverse plane, m is the ion mass, and $U(r)$ is the continuum potential at $\mathbf{r}$, in general a sum of the continuum potentials of the rows forming the two-dimensional transverse lattice. It is convenient to introduce the reduced transverse energy $\varepsilon_\perp = 2E_\perp/E\psi_1^2$, where ψ_1 is the Lindhard angle,

$$\psi_1 = \left[\frac{2Z_1Z_2e^2}{Ed}\right]^{1/2} .$$

Here, Z_1 is the atomic number of the ion, E its energy, Z_2 the atomic number of the crystal, and d the average atomic spacing in the axial row.

A beam of ions incident upon a crystal will have some distribution in transverse energy upon transmission through the surface. The process of dechanneling can then be described by the evolution of this distribution in transverse energy $g(\varepsilon_\perp,z)$ with depth according to the "diffusion" equation,[3-6]

$$\frac{\partial f(\varepsilon_\perp,z)}{\partial z} = D(\varepsilon_\perp)\frac{\partial^2 f(\varepsilon_\perp,z)}{\partial \varepsilon_\perp^2} + \Delta(\varepsilon_\perp)\frac{\partial f(\varepsilon_\perp,z)}{\partial \varepsilon_\perp} + \delta(\varepsilon_\perp)\frac{\partial f(\varepsilon_\perp,z)}{\partial \varepsilon_\perp} - \sigma(\varepsilon_\perp)g(\varepsilon_\perp,z) ,$$

where

$$f(\varepsilon_\perp,z) = g(\varepsilon_\perp,z)/A(\varepsilon_\perp) ,$$

$A(\varepsilon_\perp)$ is the fractional area of the transverse plane accessible to an ion with transverse energy $\varepsilon_\perp$, $D(\varepsilon_\perp)$ is a diffusion function discussed below, $\delta(\varepsilon_\perp)$ is a function describing the change of $\varepsilon_\perp$ due to energy loss of the ion (damping), and $\sigma(\varepsilon_\perp)$ is an absorption function which takes into account the effects of large-angle single scattering. The diffusion function is related to the rate of change with depth of the transverse energy,

$$\Delta(\varepsilon_\perp) = d\langle\varepsilon_\perp\rangle/dz ,$$

by

$$D(\varepsilon_\perp) = \frac{1}{A(\varepsilon_\perp)}\int_0^{\varepsilon_\perp} A(\varepsilon_\perp')\Delta(\varepsilon_\perp')d\varepsilon_\perp' .$$

The rate of change of transverse energy with depth can be divided[2,3] into a nuclear part $\Delta_n(\varepsilon_\perp)$, arising from scattering by the thermally fluctuating force, and an electronic part $\Delta_e(\varepsilon_\perp)$, arising from scattering by electrons in the channel, with

$$\Delta(\varepsilon_\perp) = \Delta_e(\varepsilon_\perp) + \Delta_n(\varepsilon_\perp) .$$

The backscattered yield as a function of depth is then obtained by integrating that portion of the beam able to interact with the crystal, given by the expression

$$\chi(z) = \int_0^\infty \Pi(\varepsilon_\perp)g(\varepsilon_\perp,z)dz ,$$

where the reaction function $\Pi(\varepsilon_\perp)$, discussed below, gives the probability of a backscattering event.

We discuss the various contributions to the dechanneling equation in turn. In the following, N is the atomic density of the crystal, d the axial row spacing, and u_2 the rms two-dimensional thermal vibration amplitude.

B. Potential, accessible area, and initial distribution

In order to obtain an accurate description of the channeling and dechanneling processes we have chosen to use the full two-dimensional transverse potential rather than the single-string approximation.[1] The potential is obtained from the coefficients of Doyle and Turner.[18] This, in turn, is obtained from fits to Hartree-Fock calculations and is expected to be reasonably accurate.

The Doyle and Turner potential[18] with coefficients optimized for diamond[19] is given in reduced units at room temperature by

$$U(\mathbf{r}) = \frac{2a_0}{Z_2}\sum_{i=1}^{4} a_i e^{-b_i r^2}$$

with

$$\{a\} = \{0.7765, 4.1208, 6.1835, 9.8763\} ,$$

$$\{b\} = \{1.0627, 3.4481, 13.3064, 79.2007\} ,$$

where $\mathbf{r}$ is measured in angstrom units and $a_0 = 52.9$ pm is the Bohr radius. The calculated continuum potentials for the three major axes in diamond, in units of the reduced transverse energy, are given in Fig. 2.

The accessible area $A(\varepsilon_\perp)$ and the initial transverse energy distribution $g_0(\varepsilon_\perp)$ are then given by

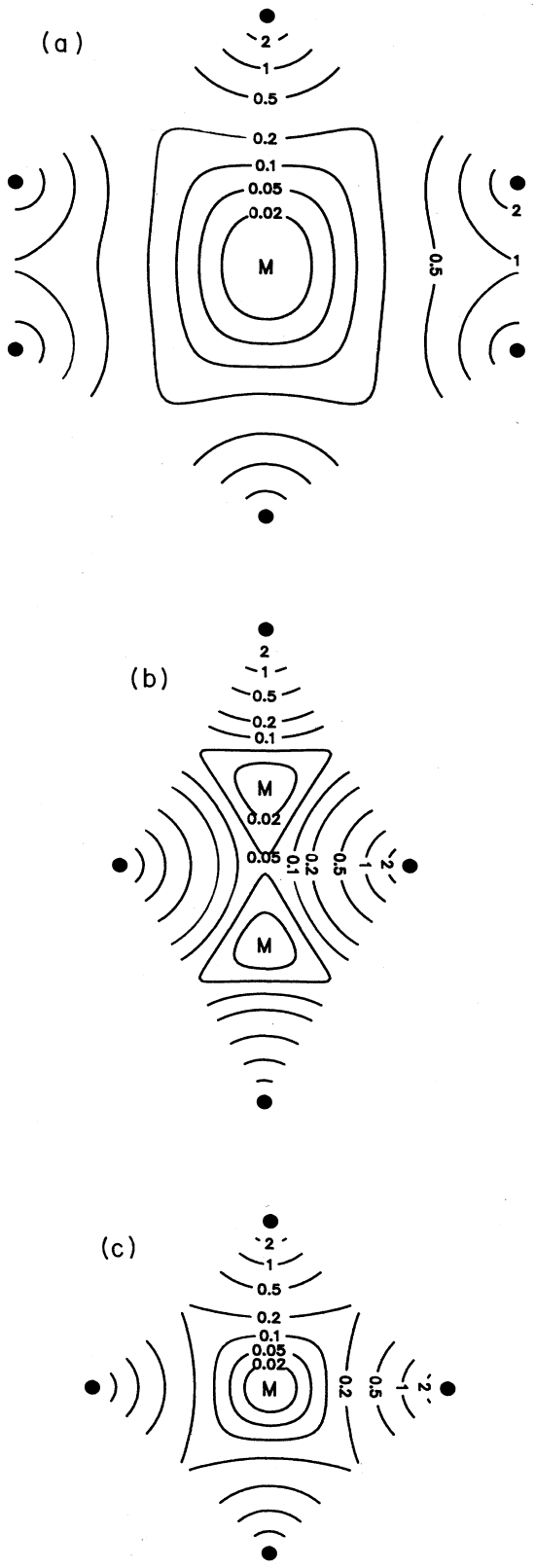

FIG. 2. Two-dimensional continuum potentials for the three major axes in diamond. The potentials are based on the Doyle–Turner potential,[11] and contours are plotted in terms of the reduced transverse energy: (a) ⟨110⟩, (b) ⟨111⟩, (c) ⟨100⟩.

$$A(\varepsilon_\perp)=\frac{1}{A_0}\int_{U(\mathbf{r})<\varepsilon_\perp} d\mathbf{r}\ ,$$

$$g_0(\varepsilon_\perp)=\frac{dA(\varepsilon_\perp)}{d\varepsilon_\perp}\ ,$$

where A_0 is the area of a unit transverse cell.

The initial distribution calculated for a multistring potential has logarithmic singularities corresponding to saddle points in the two-dimensional transverse potential.[20] In the calculation, these have been truncated to peaks because of the finite mesh used. This is not expected to have a significant effect on the yield as this is insensitive to small perturbations in the initial distribution. The initial transverse energy distributions for the three axes ⟨110⟩, ⟨111⟩, and ⟨100⟩ are given in Fig. 3. Also shown for comparison are the corresponding single-string distributions calculated with the Lindhard standard potential[1]

$$U(r)=\frac{Z_1Z_2e^2}{Ed}\ln\left[1+\frac{C^2a^2}{r^2}\right]\ ,$$

where $C^2\approx 3$ and a is the Thomas-Fermi screening radius.

C. The reaction function

The reaction function gives the probability for an ion with transverse energy $\varepsilon_\perp$ to backscatter, relative to the probability in a random medium of the same density. It is given by[1]

$$\Pi(\varepsilon_\perp)=\frac{1}{A(\varepsilon_\perp)}\int P(\mathbf{r})d\mathbf{r}\ .$$

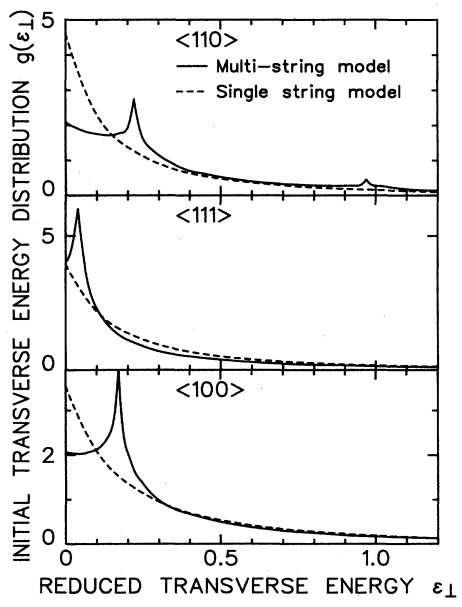

FIG. 3. Initial transverse energy distributions for the three major axes in diamond as a function of the reduced transverse energy. The solid line gives the distribution corresponding to the two-dimensional Doyle-Turner potential, and the dashed line corresponds to the single-string Lindhard potential.

Here, $P(\mathbf{r})$ is the density in the transverse plane of the thermally vibrating crystal atoms,

$$P(\mathbf{r})=\frac{1}{\pi N\, du_2^2}e^{-r^2/u_2^2}.$$

D. The nuclear and electronic scattering terms

These terms are related to the change in mean multiple-scattering angle with depth produced by the respective phenomena. The change in transverse energy with depth is then given by[1]

$$\Delta(\varepsilon_\perp)=\frac{d\varepsilon_\perp}{dz}=\frac{1}{A(\varepsilon_\perp)}\int\frac{2}{\psi_1^2}\frac{\delta\psi^2}{\delta z}(\mathbf{r})d\mathbf{r},$$

where the integral is taken over a unit transverse cell.

The nuclear term receives contributions predominantly from small impact parameter scattering events and may thus be approximated using a single-string model. The following expression has been obtained for small $\varepsilon_\perp$ (large distances from the string) for the Lindhard standard potential by Schiøtt *et al.*,[4] to second order in u_2^2/C^2a^2:

$$\Delta_n(\varepsilon_\perp)=(\gamma_1+\gamma_2)\Delta_{\text{random}},$$

where

$$\gamma_1=\frac{1}{A(\varepsilon_\perp)}\frac{1}{2L_n}\frac{u_2^2}{C^2a^2}\left[(\alpha e^{\varepsilon_\perp}+\tfrac{2}{3})\left[1-\frac{e^{\varepsilon_\perp}}{\alpha}\right]^3-(\alpha+\tfrac{2}{3})\left[1-\frac{1}{\alpha}\right]^3\right],$$

$$\gamma_2=\frac{1}{A(\varepsilon_\perp)}\frac{1}{2L_n}\frac{u_2^4}{C^4a^4}\left[\left[\alpha^2e^{2\varepsilon_\perp}-2\alpha e^{\varepsilon_\perp}-\frac{4}{\alpha}e^{-\varepsilon_\perp}-\frac{7}{\alpha^2}e^{-2\varepsilon_\perp}+\frac{26}{\alpha^3}e^{-3\varepsilon_\perp}-\frac{24}{\alpha^4}e^{-4\varepsilon_\perp}+\frac{36}{5\alpha^5}e^{-5\varepsilon_\perp}\right]-\left[\alpha^2-2\alpha-\frac{4}{\alpha}-\frac{7}{\alpha^2}+\frac{26}{\alpha^3}-\frac{24}{\alpha^4}+\frac{36}{5\alpha^5}\right]\right].$$

Here, γ_1 and γ_2 are, respectively, the first- and second-order contributions, $\alpha=1+C^2a^2/r_0^2$, where r_0 is the effective channel radius defined by $r_0=(\pi Nd)^{-1}$, and $L_n=\ln(1.29\varepsilon)$, where ε is the usual reduced energy

$$\varepsilon=\frac{a}{Z_1Z_2e^2}\frac{M_2}{M_1+M_2}E.$$

This expression has been obtained using the Lindhard potential, and has the advantage that it can be expressed in closed form. However, the choice of potential does not in fact influence this function much in the important region $\varepsilon_\perp<2$, and in Fig. 4 we show $\Delta_n(\varepsilon_\perp)$ calculated with three potentials, the Lindhard standard potential, the Moliére potential, and a potential calculated from Clementi single-ζ Hartree-Fock wave functions[21] for carbon. The function has been calculated numerically for the latter two potentials. (We note in passing that the Doyle and Turner approximation to the Hartree-Fock potential is inadequate for this purpose, as the derivatives obtained from this potential are not sufficiently accurate and lead to large oscillations in the result.) In view of this numerical agreement, and in order to avoid computational complexity, we have used the Lindhard-potential expressions in our calculations.

At larger $\varepsilon_\perp$ the nuclear scattering can be taken as proportional to the local atom density in the transverse plane, which yields

$$\Delta_n(\varepsilon_\perp)=\Delta_{n,r}\Pi(\varepsilon_\perp),$$

where $\Delta_{n,r}$ is the random value and $\Pi(\varepsilon_\perp)$ is the reaction function. The random nuclear scattering value is[1]

$$\Delta_{n,r}=\pi d^2\psi_1^2NL_n=\frac{1}{x_n}L_n.$$

The nuclear term $\Delta_n(\varepsilon_\perp)$ also contains contributions from low-probability large-angle scattering events. These contributions lead to the value for $\Delta_n(\varepsilon_\perp)$ being overestimated at large transverse energies. We thus restrict the scattering to small angles, i.e., angles less than ψ_1, and take account of large-angle scattering by means of the absorption term in the diffusion equation. With this restriction in scattering angles, the random nuclear scattering term becomes

$$\Delta_{n,r}=\frac{1}{x_n}\ln\left[1.29\varepsilon\frac{\psi_1}{2}\right].$$

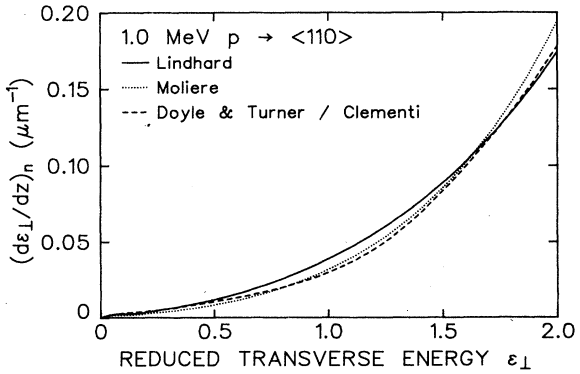

FIG. 4. Nuclear scattering function for three potentials. 1.0 MeV protons in diamond, ⟨110⟩.

From the usual impulse approximation for the scattering potential one obtains[1] the cross section for scattering through an angle larger than some ψ_c,

$$\sigma_a=\pi\left[\frac{Z_1Z_2e^2}{E}\right]^2\frac{1}{\psi_c^2}\ .$$

With $\psi_c=\psi_1$, the absorption term in the diffusion equation is then given by

$$\sigma(\varepsilon_\perp)=\sigma_d\Pi(\varepsilon_\perp)\ .$$

The full nuclear contribution was then obtained by combining the small-$\varepsilon_\perp$ and large-$\varepsilon_\perp$ approximations in the manner of Schiøtt *et al.*[4]

The electronic contribution is given by[2,3,6]

$$\Delta_e(E_\perp)=\frac{1}{A(\varepsilon_\perp)}\int_{U(r)\le\varepsilon_\perp}\frac{A(\varepsilon_\perp)\delta\psi_e^2}{\delta z}(\mathbf{r})d\mathbf{r}\ .$$

Various approximations for this function have been proposed.[1,3,5,6] These approximations are based on the use of the scattering for an ion moving through a free-electron gas; extension to the position-dependent electron density in the channel is through the local-density approximation (LDA). The approximations differ in the approximation used for the free-electron gas scattering, and in the modeling of the electron density in the channel. Most are based on the Lindhard potential.

We note that the validity of the LDA under channeling conditions has not been established, and more elaborate calculations of scattering in planar channeling have given results very different from the LDA.[22] Certain elements of the LDA, such as the use of the local electron density in the determination of the plasmon frequency (a collective quantity), are disturbing. It is apparent that the LDA expression for electron scattering is, at best, a gross approximation, and probably the most uncertain element in calculating the dechanneling of ions. Nevertheless, we are constrained, by the lack of alternatives, to use it.

In view of this, we have chosen to use the following parametrization of the function $\Delta_e(\varepsilon_\perp)$, which allows us to match several different approximations by suitable choice of the parameters α and β:

$$\Delta_e(\varepsilon_\perp)=\frac{1}{z_e}\alpha(1-\beta e^{-\varepsilon_\perp})\ .$$

Here, z_e is a characteristic length determined by the electronic stopping power and defined by

$$z_e=\frac{E}{\pi Z_1e^2L_eN\,d}\ ,$$

where

$$L_e=\frac{m_ev^2}{4\pi Z_1^2e^4NZ_2}\left[\frac{dE}{dz}\right]_e\ .$$

The two fitting constants can be chosen to reproduce the scattering at $\varepsilon_\perp=0$ and $\varepsilon_\perp\to\infty$. Typically, Δ_e varies by a factor of about 2 over this region.

The parameters have been determined by using the LDA, with the electron density at the minimum of the potential derived from the Doyle and Turner values, and the scattering calculated from the result for the free-electron gas obtained by Matsunami and Howe.[6] For the ⟨110⟩ axis, our parametrized expression for $\Delta_e(\varepsilon_\perp)$ differed from that of a full LDA calculation using the Doyle and Turner electron densities by at most 12%.

The damping term is given by[4]

$$\delta(E_\perp)=\frac{1}{A(\varepsilon_\perp)}\int[\varepsilon_\perp-U(\mathbf{r})]\frac{1}{E}\frac{dE}{dz}(\mathbf{r})d\mathbf{r}$$
$$\simeq-\beta\frac{E_\perp}{E}\left\langle\frac{dE}{dz}\right\rangle\ ,$$

with $\beta\simeq0.5$ and $\langle\cdots\rangle$ represents the average over the accessible area. The term has a rather small effect and a relatively crude approximation is justified:

$$\left\langle\frac{dE}{dz}\right\rangle=\frac{dE}{dz}\left[1-\frac{e^{-\varepsilon_\perp}}{\alpha}\right]\ ,$$

where α is chosen to match the stopping power at the channel center.

E. Solution of the dechanneling equation

The diffusion equation was solved numerically using the Crank-Nicholson method.[23] Two approaches were tried for handling the unbounded coordinate $\varepsilon_\perp$. In one, the interval $\varepsilon_\perp=0$ to ∞ was mapped into $(-1, 1)$ with the transformation

$$\tan\varepsilon_\perp=(\pi/2)y^2\ .$$

In the other approach, the transverse energy space was arbitrarily truncated at $\varepsilon_\perp=10$ by imposing the boundary condition $g(\varepsilon_\perp,10)=0$. That portion of the flux passing the boundary, given by

$$\frac{dF}{dz}=\left[A(\varepsilon_\perp)D(\varepsilon_\perp)\frac{\partial}{\partial\varepsilon_\perp}\frac{g}{A}\right]_0^{10}$$

was integrated and included in the yield. The two approaches were found to agree closely, and most calculations were performed using the second method. A check was maintained on the overall normalization defined by

$$N(z)=1+\int_0^z\left[AD\frac{\partial}{\partial\varepsilon_\perp}\frac{g}{A}\bigg|_{\varepsilon_\perp=10}+\int_0^{10}\sigma\Pi g\,d\varepsilon_\perp\right]dz'\ .$$

This did not differ from unity by more than 0.1%.

Some problems can be experienced because $A(\varepsilon_\perp)$ tends to zero as $\varepsilon_\perp\to0$. Some authors[4,6] impose a nonzero lower limit on $A(\varepsilon_\perp)$ by assuming a minimum accessible area limited by thermal vibrations. We have chosen a less arbitrary and perhaps more physical way of treating this problem. With $A(0)=0$, the transverse energy distribution at the boundary, $g(0,z)$ is forced to 0. The equation may be solved with this condition imposed from the outset. In order to have $g(0,0)=0$, we allow for a Gaussian spreading of the incident beam due to beam

divergence, and scattering from surface impurities. The initial distribution then becomes

$$g(\varepsilon_\perp,0)=\int_0^{\varepsilon_\perp}\frac{1}{\varepsilon_s}\exp\left[-\frac{\varepsilon_\perp'}{\varepsilon_s}\right]g_0(\varepsilon_\perp-\varepsilon_\perp')d\varepsilon_\perp' ,$$

where $\varepsilon_s=2\psi_s^2/\psi_1^2$ and ψ_s^2 is the variance of the Gaussian spread in incident angle. Now, since ε_s is usually small ($\psi_s \ll \psi_1^2$), and g_0 is approximately constant for small $\varepsilon_\perp$ and is relatively smooth thereafter, this integral may be approximated, without much loss in accuracy, as

$$g(\varepsilon_\perp,0)=g_0(0,0)(1-e^{-\varepsilon_\perp/\varepsilon_s}),\quad \varepsilon_\perp\le\varepsilon_c$$

$$=g_0(\varepsilon_\perp-\varepsilon_c,0)(1-e^{-\varepsilon_\perp/\varepsilon_s}),\quad \varepsilon_\perp\ge\varepsilon_c .$$

The reaction function as given above is inadequate to determine the yield correctly in that the calculated yield is too low, and also the calculated value of $\psi_{1/2}$ is greater than the experimental value.[24] The reaction function has thus been scaled so that the experimental value[24] of $\psi_{1/2}$ is matched. This leads to the value at which the reaction function reaches 0.5 being reduced in $\varepsilon_\perp$ by about 0.09 in all three axes. This effect has been commonly noted in calculations and Barrett[25] has suggested that neglect of focusing in the transverse plane is responsible. However, use of the Doyle-Turner potential usually gives good agreement between measured and calculated dipwidths, suggesting that the potential chosen for the calculation is equally important. (Barrett used the Molière potential.) It is possible that the use of the Doyle-Turner potential in diamond is inadequate without taking into account the redistribution of the valence electrons into the covalent bonds.[26]

The effect of the various terms in the diffusion calculation was determined by numerically switching off the respective functions. The effects are shown in Fig. 5 for the case of the ⟨110⟩ axis at room temperature for 1.0-MeV protons. The effect of the damping and absorption terms is small, while that of the nuclear scattering term is somewhat larger. However, it is clear that the electronic term is dominant in the theoretical calculations.

IV. RESULTS AND DISCUSSION

Energy spectra were taken with channeled and random alignment for incident proton energies of 1.0, 4.5, 7.0, and 8.9 MeV with the crystal of 20 °C. Spectra were also taken at 1.0 MeV with the crystal at temperatures of 300 and 600 °C. The yield at room temperature was determined from the energy spectra according to the procedures outlined in Sec. II and is plotted as a function of depth for the ⟨110⟩ axis in Fig. 6. This figure illustrates the energy dependence of the dechanneling over the wide range of incident energies used. The range of the data reflects the depth accessible by ions of differing energies.

Because of the theoretical dominance of the electronic scattering, it is interesting to scale the depth variable with the characteristic length for electronic scattering, z_e. The resulting plots of the yield against the scaled variable z/z_e are shown for the three major axes in Figs. 7–9, together with calculations of the yield for 1.0 and 8.9 MeV. The results indicate that the scaling of the yield is quite good for all three axes. The scaling also holds over a wide energy range. This suggests that the theoretical dominance of the electronic scattering is confirmed by the data. It must be noted, however, that the energy dependence of the nuclear term is similar to that of the electronic term, and thus some compensation will occur. The diffusion-model calculation gives good agreement with the experimental data.

The expression for z_e also contains the scaling of the electronic term from axis to axis; however, the functional dependence on $\varepsilon_\perp$ differs from axis to axis in the small-$\varepsilon_\perp$ region. At larger $\varepsilon_\perp$ the electronic scattering is determined essentially by the value for random alignment. One may therefore expect that the dechanneling behavior

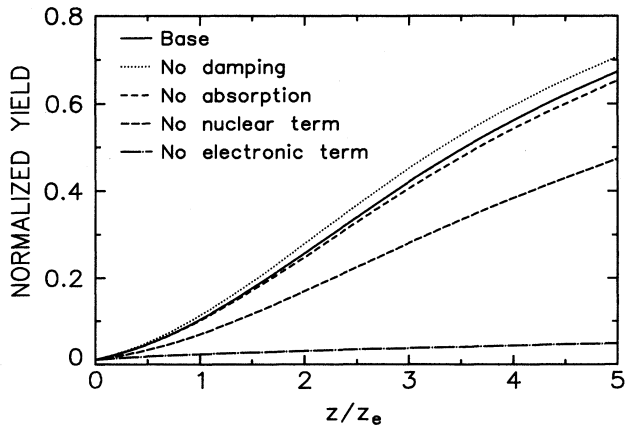

FIG. 5. Sensitivity of the dechanneled yield to various terms of the diffusion calculation.

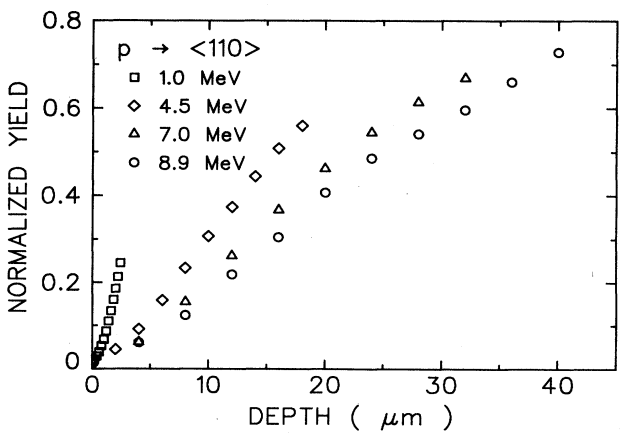

FIG. 6. Dechanneled yield of protons in diamond ⟨110⟩ as a function of depth at 1.0, 4.5, 7.0, and 8.9 MeV.

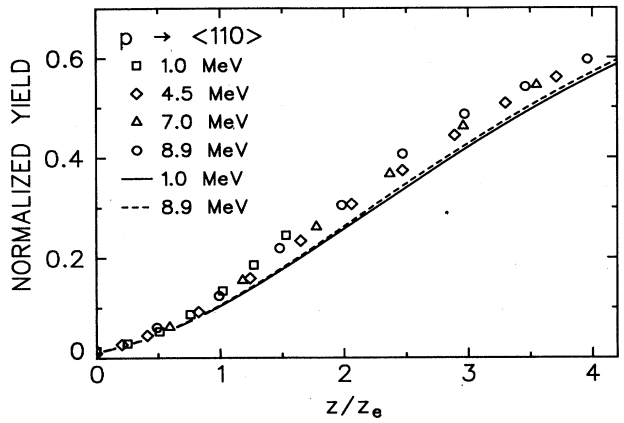

FIG. 7. Dechanneled yield as a function of reduced depth for 1.0-, 4.5-, 7.4-, and 8.9-MeV protons in diamond ⟨110⟩. The points give experimental results and the curves give the results of the calculations discussed in the text.

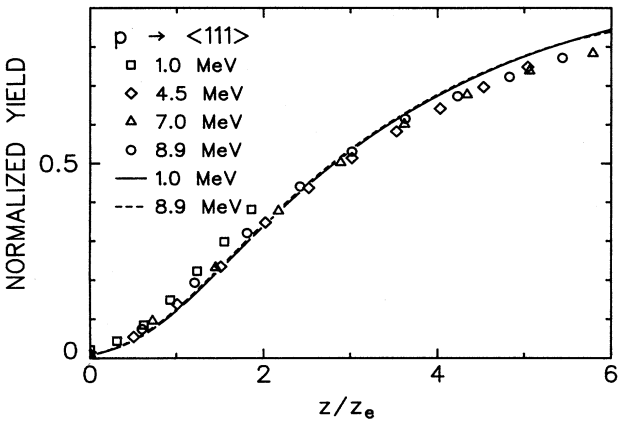

FIG. 8. Dechanneled yield as a function of reduced depth for 1.0-, 4.5-, 7.4-, and 8.9-MeV protons in diamond ⟨111⟩. The points give experimental results and the curves give the results of the calculations discussed in the text.

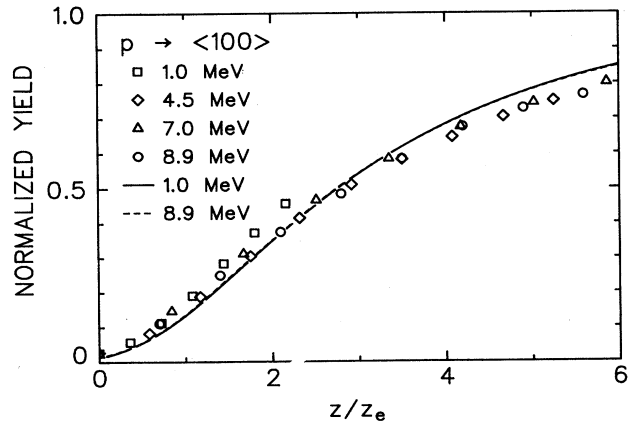

FIG. 9. Dechanneled yield as a function of reduced depth for 1.0-, 4.5-, 7.4-, and 8.9-MeV protons in diamond ⟨100⟩. The points give experimental results and the curves give the results of the calculations discussed in the text.

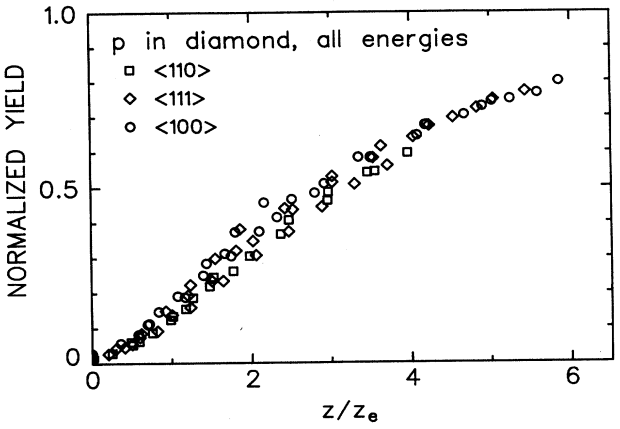

FIG. 10. Dechanneled yield as a function of depth for all axes and energies.

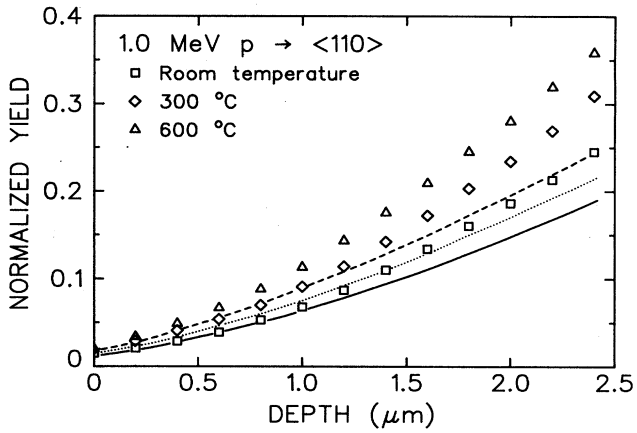

FIG. 11. Dechanneled yield as a function of temperature at 1.0 MeV for ⟨110⟩. Solid line: 20°C, dotted line: 300°C, dashed line: 600°C.

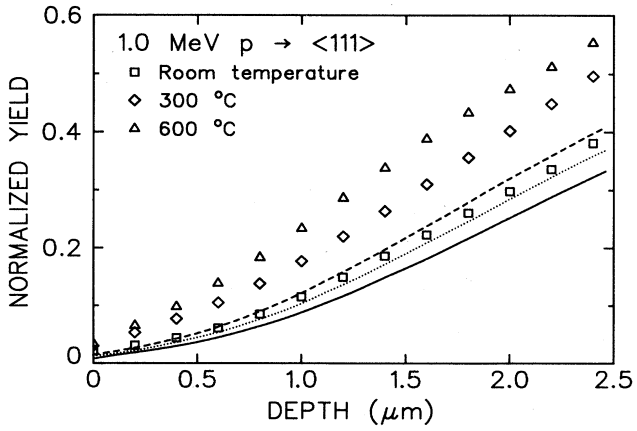

FIG. 12. Dechanneled yield as a function of temperature at 1.0 MeV for ⟨111⟩. Solid line: 20°C, dotted line: 300°C, dashed line: 600°C.

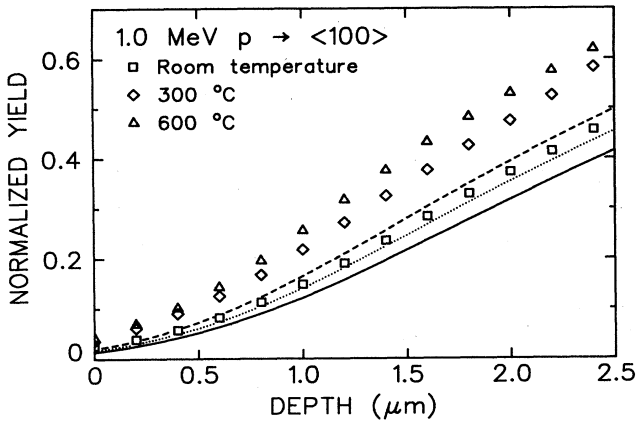

FIG. 13. Dechanneled yield as a function of temperature at 1.0 MeV for ⟨100⟩. Solid line: 20 °C, dotted line: 300 °C, dashed line: 600 °C.

all three axes should show some similarities. The experimental results for all three axes are plotted in Fig. 10. The general agreement for all three axes is remarkable, considering the wide range in axes and energy represented by the data. It is evident that the diffusive nature of the dechanneling process is responsible for smoothing out small difference in the initial distributions to produce a similar behavior at larger depths in all three cases. We conclude that, provided that one dechanneling mechanism is dominant, scaling behavior may be observed in dechanneling.

The temperature-dependent data are plotted in Figs. 11–13 together with the corresponding results from the diffusion model calculations. It is clear that the temperature dependence of the dechanneling is seriously underestimated by the calculations. The reason for this is not clear. We do not believe that a change in potential will affect the results much. It is possible that the underlying

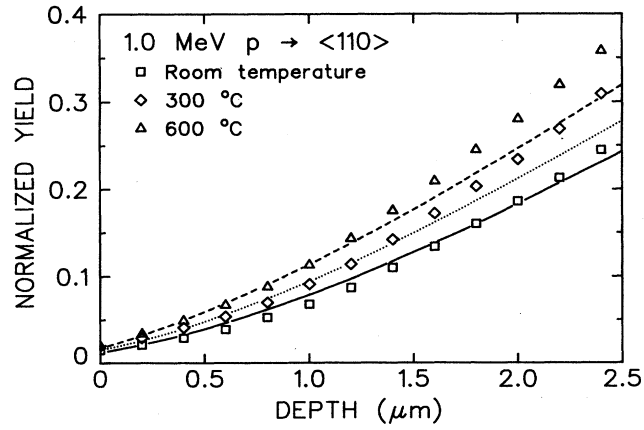

FIG. 14. Comparison of experimental and theoretical results with increased thermal term in the calculation. 1.0-MeV protons in ⟨110⟩. Solid line: 20 °C, dotted line: 300 °C, dashed line: 600 °C.

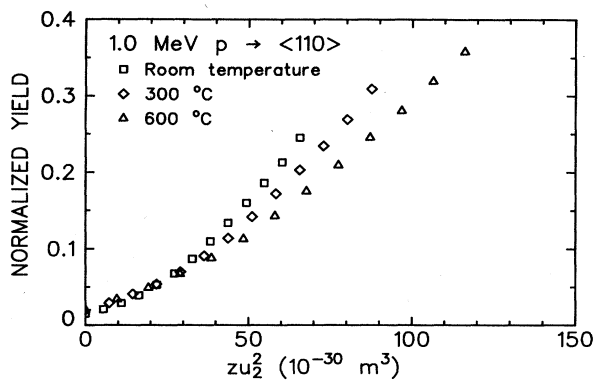

FIG. 15. Yield as a function of depth for 1.0-MeV protons in ⟨110⟩ plotted as a function of the variable zu_2^2.

model description of the thermal dechanneling contribution is inadequate. For instance, it has been suggested that focusing in the transverse plane may enhance this term. Such effects are not easy to evaluate without a Monte Carlo simulation. However, the connection of such a simulation to the dechanneling contribution is also not easily made. In order to examine the increase in the thermal term necessary to match the data, we have made calculations with the thermal term multiplied by an arbitrary factor and find an increase in u_1^2 by a factor of about 2 is needed. This factor has little effect on the room-temperature results. The resulting agreement between experiment and calculation is illustrated in Fig. 14. We note that the crystal temperatures reached in this experiment are all well below the Debye temperature of diamond. This is in contrast to the usual case with other crystals, and so comparisons may be difficult to make.

Some authors[2,8,9] have sought a scaling of temperature-dependent dechanneling data with the variable zu_2^2. We have therefore plotted the dependence of the experimental yield on the variable in Fig. 15, for the 1.0 MeV, ⟨110⟩ case. While there is a region of scaling near the origin, this does not hold for larger zu_2^2. Similar behavior has been observed by others[6,10] for silicon and germanium. We conclude that scaling with this variable also does not hold in the case of diamond.

In summary, we have measured the dechanneled yield for protons in diamond over a wide range of energy and temperature. We conclude that the diffusion model provides a good description of the dechanneling. Scaling of the yield by a suitably chosen variable allows the data from a wide range of energies and axes to be consolidated, and lends support to the theoretically based supposition that the dechanneling in diamond under the above conditions is dominated by electronic scattering.

ACKNOWLEDGMENTS

The authors acknowledge with appreciation the support of the Foundation for Research Development and of de Beers Industrial Diamonds (Pty) Ltd.

[1]J. Lindhard, K. Dansk. Vidensk. Selsk. Mat. Fys. Medd. **34**, No. 14 (1965).
[2]G. Foti, F. Grasso, R. Quatrocchi, and E. Rimini, Phys. Rev. B **3**, 2169 (1971).
[3]E. Bonderup, H. Esbensen, J. U. Andersen, and H. E. Schiøtt, Radiat. Eff. **12**, 261 (1972).
[4]H. E. Schiøtt, E. Bonderup, J. U. Andersen, and H. Esbensen, *Atomic Collisions in Solids,* edited by S. Datz, B. R. Appleton, and C. D. Moak (Plenum, New York, 1975), p. 843.
[5]V. V. Beloshitsky, M. A. Kumakhov, and V. A. Muralev, Radiat. Eff. **13**, 9 (1972).
[6]N. Matsunami and L. M. Howe, Radiat. Eff. **51**, 111 (1980).
[7]J. Field, *The Properties of Diamond* (Academic, London, 1979).
[8]S. U. Campisano, F. Grasso, and E. Rimini, Radiat. Eff. **9**, 153 (1972).
[9]S. U. Campisano, G. Foti, F. Grasso, M. LoSavio, and E. Rimini, Radiat. Eff. **13**, 157 (1972).
[10]M. J. Pedersen, J. U. Andersen, D. J. Elliot, and E. Laesggaard, *Atomic Collisions in Solids,* edited by S. Datz, B. R. Appleton, and C. D. Moak (Plenum, New York, 1975), p. 863.
[11]R. W. Fearick, T. E. Derry, and J. P. F. Sellschop, Nucl. Instrum. Methods **168**, 195 (1980).
[12]M. Rebak, J. P. F. Sellschop, T. E. Derry, and R. W. Fearick, Nucl. Instrum. Methods **167**, 115 (1979).
[13]S. D. Softky, Phys. Rev. **123**, 1685 (1961).
[14]H. H. Andersen and J. Ziegler, *Hydrogen Stopping Powers and Ranges in all Elements* (Pergamon, New York, 1977).
[15]R. W. Fearick and J. P. F. Sellschop, Nucl. Instrum. Methods. **168**, 51 (1980).
[16]S. Matteson, E. K. L. Chau, and D. Powers, Phys. Rev. A **14**, 169 (1976).
[17]G. Molière, Z. Naturforsch. **2a**, 133 (1947).
[18]P. A. Doyle and P. S. Turner, Acta Crysallogr. A **24**, 390 (1968).
[19]J. U. Andersen (private communication).
[20]J. H. Barrett, B. R. Appleton, T. S. Noggle, C. D. Moak, J. A. Biggerstaff, S. Datz, and R. Behrisch, *Atomic Collisions in Solids,* edited by S. Datz, B. R. Appleton, and C. D. Moak (Plenum, New York, 1975), p. 645.
[21]E. Clementi and C. Roetti, At. Data Nucl. Data Tables **14**, 117 (1974).
[22]H. Nitta, Y. H. Ohtsuki, and K. Kubo, Phys. Rev. B **34**, 7549 (1986).
[23]R. D. Richtmeyer and K. W. Morton, *Difference Methods for Initial Value Problems* (Wiley, New York, 1967).
[24]T. E. Derry, R. W. Fearick, and J. P. F. Sellschop, Phys. Rev. B **26**, 17 (1982).
[25]J. H. Barrett, Phys. Rev. Lett. **31**, 1542 (1973).
[26]J. U. Andersen, S. Datz, E. Laegsgaard, J. P. F. Sellschop, and A. H. Sørensen, Phys. Rev. Lett. **49**, 215 (1982).